

FIG. 70. Left hand plot shows the energy deposition from Bethe-Heitler muons *vs.* the cosine of the polar angle and azimuthal angle in the calorimeter for a 0.5 TeV CoM collider. Right hand plot shows the same distributions with a 1 ns timing cut.

## IX. DETECTOR SCENARIOS

The background consists of neutral and charged particles. For neutrons, the longitudinal and radial fluences were found to be comparable. The photons (average energy about 1 MeV) show a clear radial source. The charged particles and the photons do not all point back to the interaction point, but to the general vicinity of the IP, namely to the region where the 20 degree tungsten shield becomes thinner. The flux of secondary muons (Bethe-Heitler pairs) is mainly longitudinal.

We would expect this background to pepper the tracking volume with random hits and produce significant energy pedestals in the calorimeter cells. These effects are considered in more detail in the following sections. In general, in designing a strawman detector that must operate in a large background flux we will want to employ as many detector channels as is practical. A strawman muon collider detector design with a few times  $10^6$  non-pixel channels would seem reasonable [227]. Over the last few years, development of pixel detectors has resulted in a quantum jump in the number of electronic channels. For example, the SLD vertex detector [228] contains  $300 \times 10^6$  pixels, and similar numbers of pixels are planned for the LHC vertex detectors. Hence, a strawman muon collider vertex detector employing  $10^8 - 10^9$  pixels would seem reasonable.

### A. Silicon vertex detector schemes

From table XVI, it can be seen that the radiation damage to silicon detectors is acceptable in terms of the number of hits per year and the resultant lifetime of the detector. This prompts [227] us to consider the following options for silicon vertex detector design for the muon collider:

- Silicon drift detector. The idea, which is described in the muon collider feasibility study [44,33], is to exploit the time gap between bunch crossings by using the silicon drift detector technology [229] (see Fig. 71). Using  $50 \times 300 \mu\text{m}^2$  detectors it should be possible to obtain a resolution of a few microns in the drift direction. This would facilitate a very precise vertex detector, although questions of radiation hardness remain to be resolved for this option.
- Columnar pixels [230]. The idea is to exploit the very well localized primary vertex position by using long thin tracking pixels that point at the IP and therefore record large ionization signals only for tracks coming from the

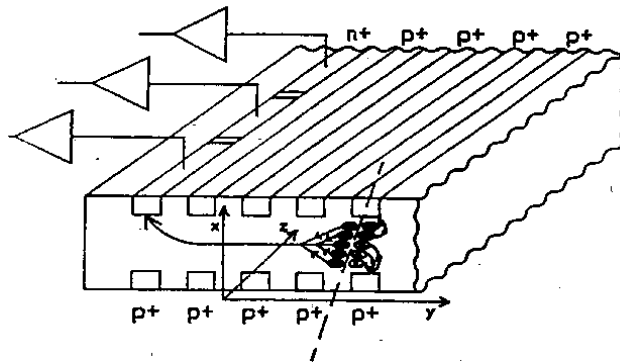


FIG. 71. Silicon drift vertex detector.

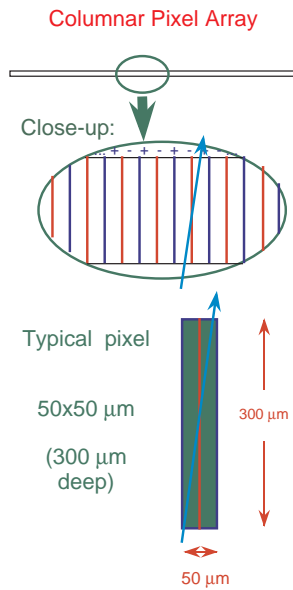


FIG. 72. Columnar pixel geometry. Courtesy of A. Sill.

IP (Fig. 72). For example, one can construct  $50 \times 50 \mu\text{m}^2$  pixels that are  $300 \mu\text{m}$  deep. The pixels are produced using controlled feed-through-drilling technology to create a lattice of anodes and cathodes that extend through the  $300 \mu\text{m}$  thick wafer.

- Pixel micro-telescopes [231]. The idea is to replace a single pixel layer with two layers separated by a small distance, and read them out by taking the AND between appropriate pairs. The distance between the layers is optimized so that soft MeV tracks (which are associated with almost 80% of the predicted background hits) produced in one layer curl up in the magnetic field before reaching the second layer. Thus, the pixel micro-telescope is blind to the soft background hits and also blind to tracks that do not come from the IP. In the example shown in Fig. 73 the top measurement layer has a finer granularity than the bottom confirmation layer. The corresponding rows in the two pixel layers can be read out with different clock speeds to maintain the correct correspondence at the input into the AND gate that registers valid hits in the telescope. If the readout rows are the ones parallel to the beam direction, then variable clock speeds can be used to maintain the correct accepted direction with respect to the IP.

The challenge of a high background environment is clearly fruitful ground for new ideas. The above considerations suggest that, provided silicon detectors can be used in the inner tracking volume, it should be possible to construct a vertex detector able to tag secondary vertices from short lived particles at a muon collider. Detailed simulations are currently underway to establish this more concretely.

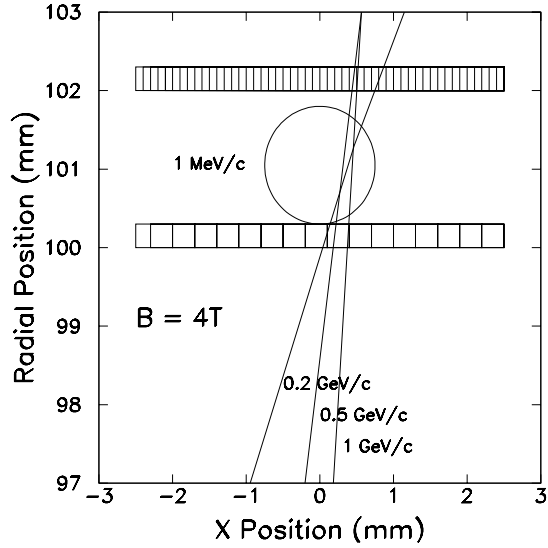


FIG. 73. Pixel micro-telescope geometry [231], showing trajectories of 0.2 GeV/c, 0.5 GeV/c, and 1 GeV/c tracks coming from the IP and bending in a 4 T field.

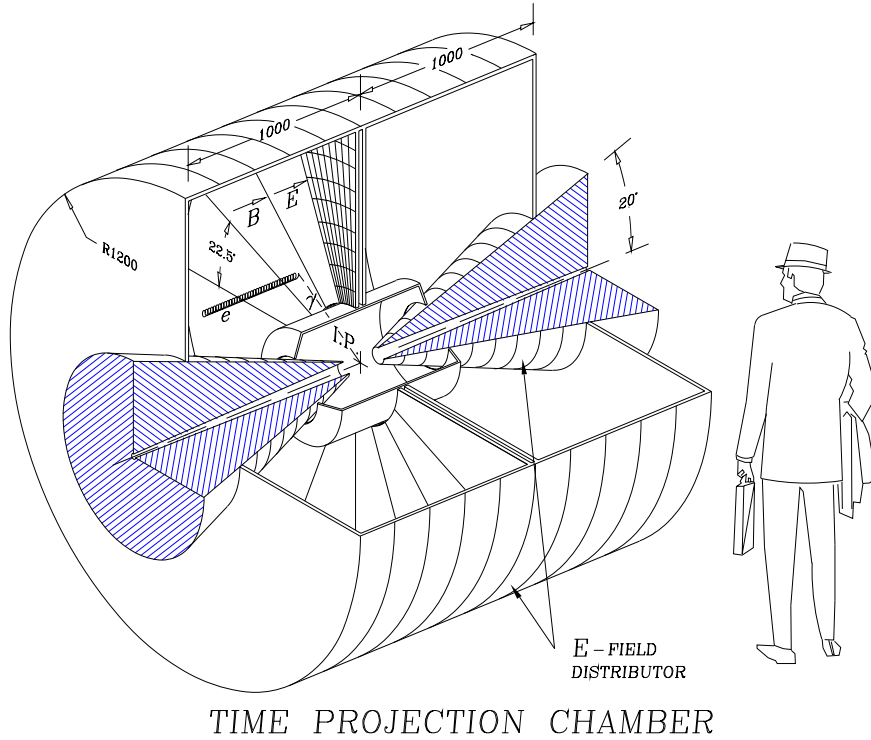


FIG. 74. Outer tracker TPC.

### B. Outer tracking schemes

The predicted background fluxes for a Higgs factory detector at a radius of 50 cm are 200 photons/cm<sup>2</sup>, 350 neutrons/cm<sup>2</sup>, and 0.08 charged tracks per cm<sup>2</sup> per crossing. The neutron flux is therefore about the same as the flux in the inner tracking volume, whereas the photon and charged particle fluxes are significantly less than those predicted at smaller radii. There are two alternative tracking strategies under consideration:

- Low field, large tracking volume drift chamber option. This option, which is described in the muon collider book [232], uses a TPC to exploit the 20  $\mu$ s time between bunch crossings. This option is viable for the very high

energy muon collider ( $1.5 \times 1.5$  TeV). The large neutron flux necessitates choosing a gas that does not contain hydrogen. A mixture of 90% neon plus 10%  $\text{CF}_4$  gives a drift velocity of  $9.4 \text{ cm}/\mu\text{s}$ , which is close to that required to match the bunch crossing time. High- $p_T$  tracks from the IP embedded in the predicted background flux have been simulated for the TPC shown in Fig. 74. The simulation includes ionization, drift and diffusion of the electrons in the gas, multiplication, and other details of the detection process. The majority of the background hits arises from low energy Compton recoils yielding very low energy electrons that have a radius of curvature of less than 1 mm in the 2 T field. Their projection on the readout plane covers not more than one readout pitch ( $0.3 \times 0.4 \text{ cm}^2$ ). These background electrons, together with the nuclear recoils from neutron scatters, yield large pulses that can be removed by cutting on the maximum acceptable pulse height. The simulation predicts that with an average background flux of  $100 \text{ photons}/\text{cm}^2$ , reasonable pulse height cuts remove only 1% of the effective TPC volume, and yield tracks of high quality. However, it was realized that positive ion build-up may be a problem with the design shown in Fig. 74. If this problem can be overcome, the design shown in the figure yields a simulated momentum resolution of about 1.2% for tracks with  $p_T = 50 \text{ GeV}/c$ .

- High field, compact silicon tracker option. An alternative strategy is to make a compact tracker by using silicon in a high field (for example, 4 T). As an example, consider the geometry shown in Fig. 75 in which a 4-layer pixel

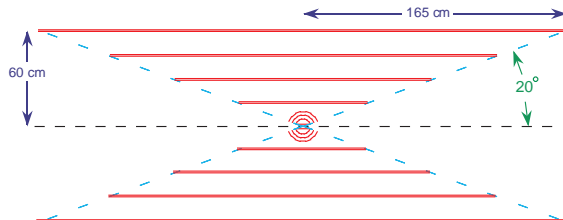


FIG. 75. Compact tracker geometry in a 4 T field.

vertex detector is surrounded by a 4-layer cylindrical stereo silicon microstrip detector. We take the inner layer of the vertex detector to consist of a cylinder of  $50 \times 300 \mu\text{m}^2$  pixels, and the outer 3 vertex layers to consist of spherical shells of  $50 \times 50 \mu\text{m}^2$  columnar pixels or pixel micro-telescopes. The resolution of the microstrip detector is chosen to match that of the pixel detector. The system is assumed to correspond to 15% of a radiation length at  $90^\circ$ . Using a parametric calculation of the momentum resolution, including multiple scattering, we obtain  $\sigma_p/p^2 = 10^{-4} (10^{-2}) (\text{GeV}/c)^{-1}$  for  $p = 100 \text{ GeV}/c$  ( $1 \text{ GeV}/c$ ).

Both the low field and high field tracking solutions look interesting and should be pursued with more complete simulations.

### C. Electromagnetic calorimeter schemes

Background particles entering the electromagnetic calorimeter are expected to give rise to significant energy pedestals in the calorimeter cells. Consider a 4 m long calorimeter that is 25 radiation lengths deep, has an inner radius of 120 cm, and is constructed from  $2 \times 2 \text{ cm}^2$  cells. This gives a total of  $10^5$  electromagnetic calorimeter towers. The GEANT background calculation predicts that each cell sees on average  $n_\gamma = 4$  background photons per crossing with a mean energy  $E_\gamma = 1 - 2 \text{ MeV}$ . If an electromagnetic shower occupies 9 cells, then the mean background pedestal will be about 70 MeV. This pedestal can be subtracted from the measured energies. The precision of the resulting electron and photon energy measurements will depend on the fluctuations in the mean background energy per cell. For an electromagnetic shower occupying 9 cells, the fluctuations in the pedestals are predicted to be about 10 MeV. This takes into account the fluctuations in the number and the energies of the background photons.

### D. Hadronic calorimeter schemes

None of the energy generated by background photons in the electromagnetic calorimeter is expected to penetrate into the hadronic calorimeter. GEANT calculations show that the total kinetic energy deposited by neutrons in the calorimeter is of the order of 140 TeV with an average energy of 30 MeV per neutron per crossing for the 4 TeV CoM energy case. In order to estimate what fraction of the kinetic energy of the neutrons will be visible, we should consider the materials involved. For this simulation we have presumed an equal mix by volume of liquid argon (as

active medium) and copper (as absorber). At 30 MeV we expect only a small fraction of the neutrons to knock off protons and only about 10% of the proton ionization to be visible in the liquid. Presuming a hadronic calorimeter with  $10^4$  towers, with the material composition described above, the average energy read in the liquid argon will be of the order of 10 MeV per tower with a fluctuation of 5 MeV. In summary, a  $50 \times 50$  GeV collider with  $4 \times 10^{12}$  muons per bunch, the photons and neutrons are expected to generate pedestals of 800 and 100 GeV respectively. The estimates for pedestal fluctuations are at or below the level of the expected electronic noise. Therefore we believe that the subtraction of these pedestals would present little problem both for the electromagnetic and the hadronic calorimeters. The presence of the high neutron background should be taken into account in choosing materials for calorimetry. Liquid argon seems a natural choice for the electromagnetic calorimeter.

The energy deposited by the Bethe-Heitler muons in the calorimeter is given in table XVII as a function of the center of mass energy of the collider. For low center of mass energies, such as the Higgs factory, the Bethe-Heitler muons are not a problem, since there are fewer of them and they leave less energy by catastrophic bremsstrahlung in the calorimeter. For the higher energy option (4 TeV in the CoM or higher), one should explore ways to correct for the energy deposition in the calorimeter, such as pattern recognition of the muon tracks or by using timing information.

### E. Muon detector schemes

The predicted background flux is expected to be relatively modest beyond a radius of 3 m in the vicinity of the muon detector. Several possible technologies for muon detectors at a muon collider were discussed during Snowmass [33]:

- Cathode strip chambers. The idea, which is described in the muon collider book [232], is to use MWPCs with segmented cathodes and a short (35 ns) drift time to provide prompt signals for triggering. The precision of the coordinate measurements would be expected to be of order  $50 \mu\text{m} \times$  a few mm.
- Threshold Cherenkov counter. The idea is to use a gas Cherenkov radiator to exploit the directionality of Cherenkov radiation in order to select high- $p_T$  muons coming from the IP. The device would also give excellent timing resolution (of order 2 ns).
- Long drift jet chamber with pad readout [233] (Fig. 76). Drift time provides the  $z$  coordinate, and pad readout provides the  $r$ - $\phi$  coordinates. Directionality at the trigger level is provided by the pattern of pad hits within a limited time window. The drift field is provided by cathode strips on grooved G-10 plates. Using 90% argon plus 10%  $\text{CF}_4$  and a maximum drift distance of 50 cm, the maximum drift time is  $5 \mu\text{s}$ .

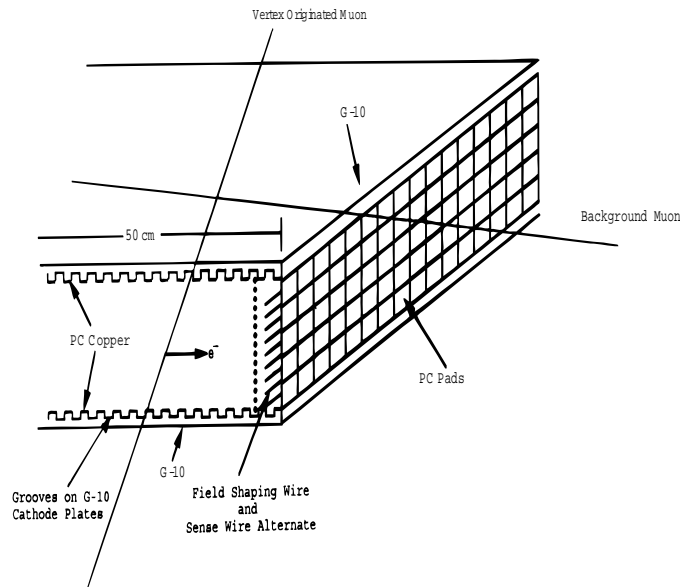


FIG. 76. Long drift jet chamber with pad readout for muon detection at a muon collider.

At high energy in the CoM, the channel  $\mu^+\mu^- \rightarrow \mu^+\mu^- + \text{Higgs boson}$  becomes particularly attractive to study using the muon collider, if the forward going muons from the interaction can be detected [234]. The method provides

a capability to search for any missing neutral state such as the Higgs boson via the missing mass technique. We are investigating methods to improve our forward muon detection capability.

## X. CONCLUSIONS

Unlike protons, muons are point-like but, unlike electrons, they emit relatively little synchrotron radiation and therefore can be accelerated and collided in rings.

Another advantage resulting from the low synchrotron radiation is the lack of beamstrahlung and the possibility of very small collision energy spreads. A beam energy spread of  $\Delta E/E$  of 0.003% is considered feasible for a 100 GeV machine. It has been shown that by observing spin precession, the absolute energy could be determined to a small fraction of this width. These features become important in conjunction with the large s-channel Higgs production ( $\mu^+\mu^- \rightarrow h$ , 43000 times larger than for  $e^+e^- \rightarrow h$ ), allowing precision measurements of the Higgs mass, width and branching ratios. A higher energy muon collider can also distinguish the nearly degenerate heavy Higgs bosons  $H^0$  and  $A^0$  of the minimal supersymmetric extension of the standard model, since these states can also be produced in the s channel. We have also examined the ability of the muon collider to study techni-resonances, do a high luminosity study of Z boson physics, scan the W and  $t\bar{t}$  thresholds to make precision mass measurements as well as SUSY and strongly interacting W boson physics. The high luminosity proton driver and the cold low energy muons permit the study of rare kaon and muon decays. Muon storage rings will permit low-systematics studies of neutrino oscillations for a wide range of mixing angle and  $\delta m^2$  phase space with hitherto unattainable sensitivity.

Such machines are clearly desirable. The issues are:

- whether they can be built and physics done with them
- what they will cost.

Much progress has been made in addressing the first question and the answer, so far, appears to be yes. It is too early to address the second.

We have studied machines with CoM energies of 0.1, 0.4 and 3 TeV, defined parameters and simulated many of their components. Most recent work has been done on the 0.1 TeV *First Muon Collider*, the energy taken to be representative of the actual mass of a Higgs particle. A summary of progress and challenges follows:

*a. Proton driver* The specification of the proton driver for the three machines is assumed the same:  $10^{14}$  protons/pulse at an energy above 16 GeV and 1-2 ns *rms* bunch lengths. There have been three studies of how to achieve these parameters. The most conservative, at 30 GeV, is a generic design. Upgrades of the FNAL (at 16 GeV) and BNL (at 24 GeV) accelerators have also been studied. Despite the very short bunch requirement, each study has concluded that the specification is attainable. Experiments are planned to confirm some aspects of these designs.

*b. Pion production and capture* Pion production has been taken from the best models available, but an experiment (BNL-E910) that has taken data, and is being analyzed, will refine these models. The assumed 20 T capture solenoid will require state-of-the-art technology. Capture, decay and phase rotation have been simulated, and have achieved the specified production of 0.3 muons per initial proton. The most serious remaining issues for this part of the machine are:

- The nature and material of the target: The baseline assumption is that a liquid metal jet will be used, but the effects of shock heating by the beam, and of the eddy currents induced in the liquid as it enters the solenoid, are not yet fully understood.
- The maximum rf field in the phase rotation: For the short pulses used, the current assumptions would be reasonably conservative under normal operating conditions, but the effects of the massive radiation from the nearby target are not known.

Both these questions can be answered in a target experiment planned to start within the next two years at the BNL AGS.

Polarization of the muon beams represents a significant physics advantage and is an important feature of a muon collider. Polarized muon beams are possible. Muons are produced with 100% polarization in the rest frame of the pion, but they travel in all directions. By accepting the forward going muons, it is easy to obtain 25% polarization in either beam easily. The amount of polarization can be increased with an accompanying price in luminosity.